

## Article

# Joint Forecasting Method of Wind and Solar Outputs Considering Temporal and Spatial Correlation

Ziran Yuan <sup>1</sup>, Pengli Zhang <sup>2</sup>, Bo Ming <sup>1</sup>, Xiaobo Zheng <sup>1,\*</sup> and Lu Tian <sup>1</sup>

<sup>1</sup> School of Water Resources and Hydroelectric Engineering, Xi'an University of Technology, Xi'an 710048, China; miloyuan1202@gmail.com (Z.Y.)

<sup>2</sup> Hanjiang-to-Weihe River Valley Water Diversion Project Construction Co., Ltd., Xi'an 710024, China

\* Correspondence: zhengxbb@163.com

**Abstract:** In response to the problem of low forecasting accuracy in wind and solar power outputs, this study proposes a joint forecasting method for wind and solar power outputs by using their spatiotemporal correlation. First, autocorrelation analysis and causal testing are used to screen the forecasting factors. Then, a convolutional neural network–long short-term memory (CNN-LSTM) is constructed and trained to extract features effectively. Finally, the independent, ensemble, and joint forecasting effects are compared, using a certain clean energy base as the research object. Results show that the forecasting accuracy of the ensemble wind and solar power outputs is better than that of independent forecasting. The joint forecasting method can improve the forecasting accuracy of wind power by 20% but slightly affects the forecasting accuracy of solar power.

**Keywords:** wind and solar power output forecasting; temporal and spatial correlation; CNN-LSTM; ensemble forecasting; joint forecasting



**Citation:** Yuan, Z.; Zhang, P.; Ming, B.; Zheng, X.; Tian, L. Joint Forecasting Method of Wind and Solar Outputs Considering Temporal and Spatial Correlation. *Sustainability* **2023**, *15*, 14628. <https://doi.org/10.3390/su151914628>

Academic Editors: Mohamed A. Mohamed and Grigorios L. Kyriakopoulos

Received: 6 September 2023

Revised: 5 October 2023

Accepted: 5 October 2023

Published: 9 October 2023



**Copyright:** © 2023 by the authors. Licensee MDPI, Basel, Switzerland. This article is an open access article distributed under the terms and conditions of the Creative Commons Attribution (CC BY) license (<https://creativecommons.org/licenses/by/4.0/>).

## 1. Introduction

Wind and solar energy are set to become the mainstay of a new type of power system, and their proportion in the energy structure increases as the energy structure transforms toward green and low-carbon sources [1]. However, influenced by various stochastic factors, such as weather and seasonal changes, the power outputs of wind and solar energy display significant random fluctuations. Directly connecting them to the grid can lead to profound impacts on the power system, resulting in issues such as voltage fluctuations, abnormal power equipment operation, and grid frequency instability [2]. Enhancing the forecasting accuracy of wind and solar power outputs plays a crucial role in ensuring the safety, stability, and economical operation of the new power system.

Forecasting methods for wind and solar power outputs can be primarily categorized into deterministic and uncertainty approaches. Deterministic methods yield predicted values based on various forecasting perspectives and spatial scales. By contrast, uncertainty forecasting employs probability density or interval probabilities to delineate the upper and lower bounds of power outputs alongside probabilities for different forecasting values [3–5]. Based on the construction process perspective of the forecasting model, commonly employed forecasting models encompass physical and data-driven models. Physical models rely on the principles of physics. They employ modeled atmospheric circulation and meteorological factors to predict outputs. Conversely, data-driven models leverage extensive historical data analysis and processing to establish mapping relationships between forecasted variables and influencing factors, enabling accurate forecasting of wind and solar power outputs [6]. In recent years, forecasting models based on deep learning have become a research hotspot [7–9]. For instance, Cui et al. [10] integrated extreme wind power fluctuation events as inputs for long short-term memory (LSTM) networks. Similarly, Zulfiqar et al. [11] introduced self-attention mechanisms to optimize feature selection in solar power output forecasting. Both studies optimize the forecasting

model from the model-building perspective. Demsew et al. [12] introduced error correction factors as innovative fuzzy input variables. They proposed a novel fuzzy particle swarm optimization model to elevate forecasting accuracy. Likewise, Liu et al. [13] found that the precision of solar power output forecasting can be enhanced by approximately 5% with the aid of high-quality contextual embeddings and gated recurrent neural networks. Wang et al. [14] noted that augmenting available time series data leads to proportional improvements in forecasting accuracy.

Given the inability of a singular deterministic forecasting model to capture the uncertainty inherent in forecasting, scholars employed methods such as probabilistic forecasting and interval forecasting to quantify the uncertainty in wind and solar power forecasting. For instance, Yang et al. [15] and Zhang et al. [16] utilized the copula quantile regression model and nonparametric probabilistic forecasting method, respectively, to describe the uncertainty in wind power outputs. Moreover, researchers introduced novel models and techniques for uncertainty forecasting [17,18] to enhance the reliability and accuracy of forecasting by characterizing and quantifying the uncertainty associated with wind and solar power generation. Yu et al. [19] introduced the Parzen window approach to estimate the error distribution in forecasting and determine the minimum confidence interval for optimal interval forecasting of wind farms. He et al. [20] combined conditional quantiles with the Epanechnikov kernel function to achieve probability density forecasting for wind and solar power outputs. These studies offer fresh perspectives and methodologies to mitigate the uncertainty in wind and solar power generation. Thus, they contribute to a comprehensive understanding of the field.

Existing research mainly focuses on the individual forecasting of renewable energy sources. However, given the correlations between different sources, practical scenarios involving multi-energy complementary scheduling often necessitate joint forecasting of various renewable energy sources [21]. Some scholars employed correlation coefficients and graphical analysis methods [22] to investigate the spatiotemporal correlations of wind and solar resources, especially the correlation between wind and solar energy. On one hand, these two renewable energy sources have low costs and rapidly increasing installed capacities. On the other hand, they exhibit a natural complementarity, making it crucial to consider the correlation between wind and solar energy when considering joint forecasting. Furthermore, they proposed complementary evaluation metrics based on the volatility of wind and solar power outputs [23,24]. These studies underscore the existence of spatiotemporal correlations between wind and solar resources. Consequently, considering the spatiotemporal correlations among different energy sources becomes essential for conducting joint power output forecasting.

Currently, some scholars have conducted joint forecasting research. For instance, Murli et al. [25] proposed a joint probability model and an optimal random forest algorithm based on meteorological data to address the uncertainty and randomness of solar and wind energy, thereby improving the performance of fault detection, classification, and regional recognition. Raksha et al. [26] established a mathematical model based on physical principles and statistical methods for jointly forecasting the uncertainty of photovoltaic generation and outdoor temperature. Zhang et al. [27] considered the spatiotemporal correlation of wind and solar resources within a region and constructed a joint prediction model that reflects the spatiotemporal correlation of regional renewable resources using attention neural network algorithms.

Building upon the previous research discussed in the preceding paragraph, this study aims to address the forecasting of wind and solar power outputs, with particular attention to their spatiotemporal correlations. Leveraging a dimensionality expansion technique built upon conventional time series predictor variables, we propose a distinctive approach to joint forecasting. Through meticulous validation with concrete examples, we seek to elucidate the uniqueness, theoretical soundness, and practical effectiveness of this method in the domain of wind and solar power output prediction. This approach not only extends existing

research but also emphasizes a comprehensive consideration of spatiotemporal correlations, thereby significantly enhancing the accuracy of wind and solar power output forecasting.

## 2. Model and Methods

In this paper, we primarily focused on the study of solar PV. A joint forecasting approach is proposed to forecast wind and solar power outputs for the following day. To simplify our modeling approach, we make several key assumptions:

1. We solely consider the resource supply side and do not incorporate aspects related to the power grid, including grid stability, demand-side management, and grid integration issues.
2. We do not take into account equipment failures, aging, or maintenance-related issues in our forecasting model. Our analysis is based on the assumption of ideal system conditions.
3. Our forecasting model relies on meteorological data such as wind speed, solar irradiance, and temperature to calculate wind and solar power outputs. Extreme weather conditions or unusual events are not considered in our analysis.
4. We calculate power outputs based on ideal conditions and do not consider constraints related to minimum wind speeds required for turbine operation or other operational limitations.

These assumptions serve as the foundation for our forecasting model and provide essential context for interpreting our results. In consideration of these assumptions, the technical process is depicted in Figure 1. First, forecasting factors for wind and solar power outputs are selected through correlation analysis. This screening process entails autocorrelation analysis and causal testing of the output sequences, culminating in the identification of a forecasting factor set with pronounced influence on the forecasting target. Subsequently, a convolutional neural network–long short-term memory (CNN-LSTM) network is constructed to harness the extraction capabilities of spatiotemporal relationships to the fullest extent. Finally, the forecasted results are analyzed to validate the efficacy and applicability of the method.

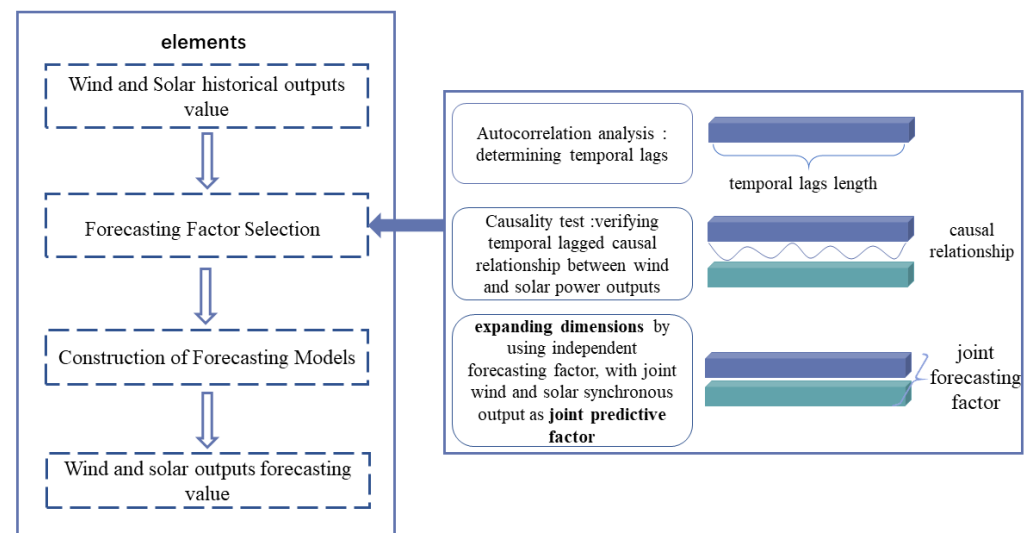


**Figure 1.** Joint forecasting flowchart.

### 2.1. Forecasting Factor Selection

Optimal forecasting factors are selected through autocorrelation analysis and joint causal testing. The Autocorrelation Function (ACF) is employed to assess temporal lags in the time series [28]. The partial ACF(PACF) is introduced to measure the correlation between the current and future lags and eliminate the influence of intermediary variables. Thus, the appropriate lag value ( $L$ ) can be determined.

Furthermore, the Granger causality test is employed to explore the interdependence and causal relationship between wind power and solar power outputs [29]. After the hypothesis formulation, the lag order for the Granger causality test statistic is determined based on ACF computation results. The calculation process is outlined as follows:

$$F_{n,p} = \frac{(n-p-1)}{p+1} \times \frac{\sum_{i=1}^{n-p} \varepsilon_i^2}{\sum_{i=1}^n \varepsilon_i^2} \quad (1)$$

where  $n$  represents the length of the time series,  $p$  signifies the lag order for the Granger causality test,  $\varepsilon_i$  denotes the residual of the  $i$ -th sample point, and  $F_{n,p}$  denotes the test statistic for the causality test, following an F-distribution with degrees of freedom  $(p+1, n-p-1)$ . The corresponding  $p$ -value is derived using the computed Granger causality test statistic, coupled with parameters such as sample size and degrees of freedom. The determination is made based on the set  $p$ -value and significance level.

After autocorrelation analysis and joint causal testing, the forecasting factors for each scenario are ascertained.

## 2.2. Construction of Forecasting Models

The establishment of independent forecasting models serves as the foundation for ensemble or joint forecasting. The groundwork is laid for the development of the joint forecasting model by constructing reliable, independent forecasting models.

### 2.2.1. Independent Forecasting

For the wind power output at time  $t$ , denoted as  $y_{t,w}$ , the preceding data of the output for the last  $L$  time steps i.e.,  $\{y_{t-1,w}, y_{t-2,w}, y_{t-3,w} \cdots y_{t-(L-1),w}, y_{t-L,w}\}$ , are employed as forecasting factors. Then, these factors are used to train a CNN-LSTM that fits the mapping function  $f$  and forecast the wind power output  $y_{t,w}$  at time  $t$ . The wind power output can be expressed as

$$y_{t,w} = f \left( \begin{array}{c} y_{t-h-1,w}, y_{t-h-2,w}, y_{t-h-3,w} \cdots \\ y_{t-h-(n-2),w}, y_{t-h-(n-1),w}, y_{t-h-n,w} \end{array} \right) \quad (2)$$

Specific adjustments are implemented when predicting solar power generation to address the issue of zero power output during nighttime. For any valid output time  $t$  denoted as  $y_{t,s}$  for solar power, the effective solar power data within the preceding  $L$  time steps, i.e.,  $\{y_{t-h-1,s}, y_{t-h-2,s}, y_{t-h-3,s} \cdots y_{t-h-(n-1),s}, y_{t-h-n,s}\}$ , are employed as forecasting factors. The formula can be expressed as

$$y_{t,s} = f \left( \begin{array}{c} y_{t-h-1,s}, y_{t-h-2,s}, y_{t-h-3,s} \cdots \\ y_{t-h-(n-2),s}, y_{t-h-(n-1),s}, y_{t-h-n,s} \end{array} \right) \quad (3)$$

where  $n$  represents the number of moments within the preceding  $L$  time steps with effective solar power output, denoting how many hours during a day have a power output greater than zero, and  $h$  signifies the number of instances with zero power output. It follows that  $L = n + h$ , as illustrated in Figure 2.

After the solar power output at time  $t$  is computed using Equation (3), it is appended to the end of the existing historical solar power data sequence. Thus, a new input sequence, which is then subjected to a sliding window forecasting approach for day-ahead forecasting, is formed.

A single forecasting value is obtained during each forecasting iteration. This forecasted value is subsequently appended to the end of the original power output data sequence. Then, the sliding window is shifted forward by one time step to update the data within the window. Subsequently, the forecasting for the next time step is made using the updated window. This process continues iteratively until the desired day-ahead forecasting length is achieved.

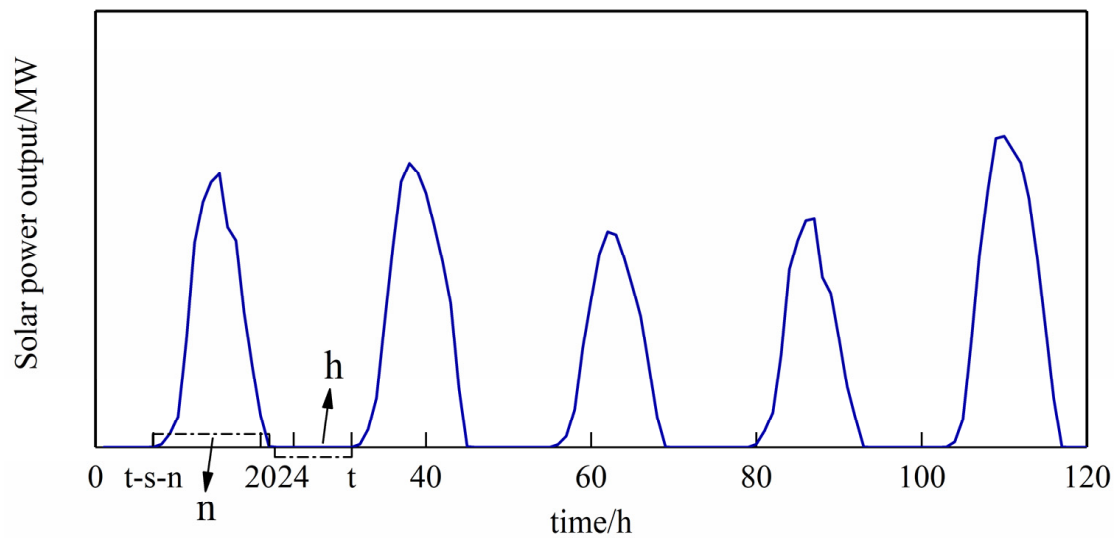


**Figure 2.** Sketch of solar forecasting input.

### 2.2.2. Ensemble Forecasting

When the ensemble forecasting model is utilized, the forecasting factors transition from individual outputs in the base model to the total output. For a given time  $t$ , the total output follows the following relationship:

$$y_{t,total} = y_{t,w} + y_{t,s} \quad (4)$$

The mathematical expression for the ensemble forecasting model at that particular time is as follows:

$$y_{t,total} = f(y_{t-1,total}, y_{t-2,total} \cdots y_{t-23,total}, y_{t-24,total}) \quad (5)$$

### 2.2.3. Joint Forecasting

In joint forecasting, the combination of wind and solar power outputs is employed as input forecasting factors, transforming the forecasting factors from a single dimension to two dimensions. For the wind power output at time  $t$ , denoted as  $y_{t,w}$ , the dimension is augmented based on the length of the independent wind power forecasting factors, and the solar output of the same period is considered. At this time, the mathematical expression of the prediction model is modified as

$$y_{t,w} = f \left[ \begin{array}{l} (y_{t-1,w}, y_{t-2,w}, y_{t-3,w} \cdots y_{t-23,w}, y_{t-24,w}), \\ (y_{t-1,s}, y_{t-2,s}, y_{t-3,s} \cdots y_{t-23,s}, y_{t-24,s}) \end{array} \right] \quad (6)$$

An extension is performed based on the length of independent solar power forecasting factors for the solar power output at time  $t$ , denoted as  $y_{t,s}$ , and given the effective solar power output. Then, the joint forecasting model is modified to

$$y_{t,s} = f \left[ \begin{array}{l} (y_{t-h-1,w}, y_{t-h-2,w}, \cdots y_{t-h-n+1,w}, y_{t-h-n,w}), \\ (y_{t-h-1,s}, y_{t-h-2,s}, \cdots y_{t-h-n+1,s}, y_{t-h-n,s}) \end{array} \right] \quad (7)$$

## 2.3. Constructing and Training the Forecasting Network

In this study, a CNN-LSTM is constructed and trained. This choice was based on our understanding of existing research and technology, and it was made after careful consideration. Previous studies have shown significant advantages of CNN-LSTM models in processing spatiotemporal data. This type of model efficiently captures spatiotemporal features in the data, demonstrating good generalization abilities and the capacity to handle complex spatiotemporal relationships. The construction of the model involves three key steps: initially, spatial features within the sequence are extracted using a convolutional

neural network (CNN). Subsequently, an LSTM layer is employed to learn the temporal dependencies within the sequence. Finally, a fully connected layer is used to map the model's output to the target forecasting variable.

### 2.3.1. CNN

In time series forecasting for wind and solar power outputs, CNN has garnered significant attention because of its exceptional feature extraction capabilities. CNNs are adept at uncovering latent correlations within historical data and transforming them into informative feature vectors. Therefore, for such problems, one-dimensional CNNs (1D-CNNs) are widely adopted for extracting output features and supporting forecasting tasks. Leveraging the power of 1D-CNNs enables the automatic capture of temporal characteristics within wind and solar power output sequences, thereby enhancing the accuracy and robustness of the forecasting model [30].

### 2.3.2. LSTM Recurrent Neural Network

The intricacies and temporal nature of wind and solar power output sequences make LSTM an ideal forecasting model [31]. LSTM learns from the historical data of a sequence to discover patterns and trends within it by using these insights to predict future output values.

Given the challenges that CNN faces in capturing long-term dependencies and LSTM's ability to extract effective features, a combination of CNN and LSTM can be beneficial. CNN can be employed as a preprocessing step to transform the raw sequence into a feature sequence. This feature sequence is then passed to LSTM to acquire a profound representation of sequence features. The schematic structure is illustrated in Figure 3.

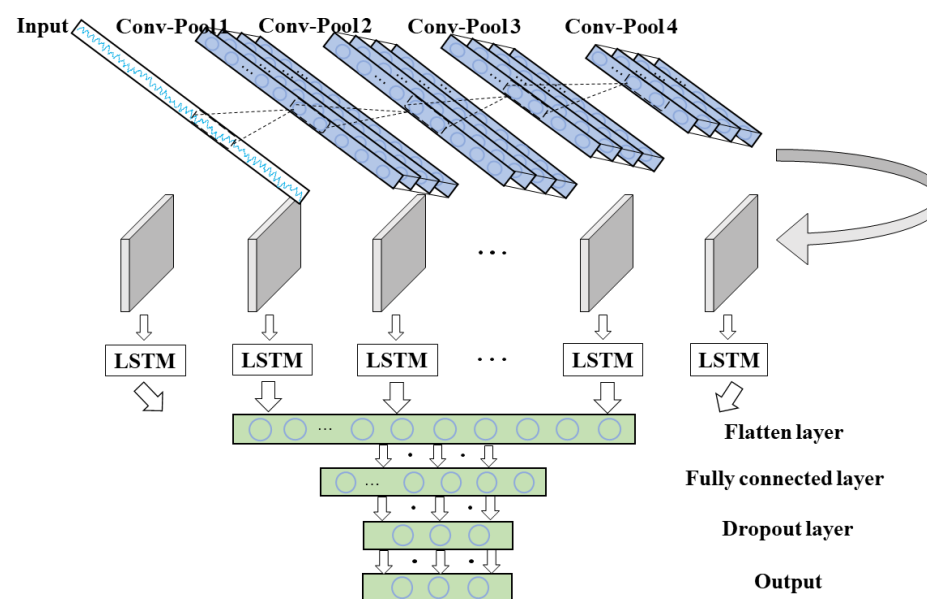


**Figure 3.** Schematic of the CNN-LSTM structure.

The input features go through a series of convolution and pooling layers, forming a 1D-CNN layer designed to extract features from wind and solar power output. Following the pooling layer, an LSTM layer is introduced to capture the spatiotemporal correlations of the output sequence. Finally, between the fully connected layer and the classification layer, a dropout layer is added to randomly deactivate some neurons, enhancing the model's robustness and generalization performance. Specific parameters are selected following a broad strategy, with the selection range shown in Table 1.

**Table 1.** Hyperparameter selection range.

Hyperparameters	Range/Value/Function	Hyperparameters	Range/Value/Function
Number of Convolutional Layers	[1, 5]	Number of LSTM Layers	[1, 2]
Convolutional Kernel Size	[1, 8]	Number of Neurons in LSTM Layers	{32, 64, 128, 256, 512}
Number of Convolutional Kernels	{32, 64, 128, 256, 512}	Number of Fully Connected Layers	[1, 2]
Padding Method	{valid, same}	Number of Neurons in Fully Connected Layers	{32, 64, 128, 256, 512}
Dropout Rates	[0, 0.9]	Learning Rates	$\{1 \times 10^2, 1 \times 10^3, 1 \times 10^4\}$

To expedite the optimization process, we set the search ranges for the number of convolutional filters, LSTM layers, and the number of neurons in the fully connected layers to common values found in typical network architectures. Additionally, we used a step size of 0.05 for the dropout rate and a step size of 1 for other hyperparameters. For the padding method, ‘valid’ signifies no zero-padding during convolution, while ‘same’ indicates zero-padding is applied. The learning rates were explored within the ranges of  $1 \times 10^2$ ,  $1 \times 10^3$ , and  $1 \times 10^4$ .

After broad strategy selection, the results of hyperparameters are shown in Table 2.

**Table 2.** Hyperparameter results.

Hyperparameters	Value/Function			
	Layers	Number of Convolutional Layers	Convolutional Kernel Size	Padding Method
Convolutional Layers	The first layer	512	6	same
	The second layer	64	1	same
	The third layer	32	6	same
	The fourth layer	128	5	valid
Number of Neurons in LSTM Layers		128		
Number of Neurons in Fully Connected Layers		128		
Dropout Rates		0.45		
Optimizer		Adam		
Learning Rates		0.0001		

#### 2.4. Forecasting Accuracy Evaluation Metrics

Given the presence of zero outputs in solar power output sequences, the R square ( $R^2$ ), mean absolute error (MAE), root mean square error (RMSE), and relative absolute error (RAE) are adopted as evaluation metrics.  $R^2$  indicates the fitting degree of the model to observed data, MAE and RMSE measure the absolute magnitude of forecasting errors, and RAE quantifies relative errors.

The accuracies of different forecasting approaches can be understood and compared by assessing these metrics comprehensively. The specific calculation formulas are as follows:

$$R^2 = 1 - \frac{\sum_{i=1}^n (p_i - a_i)^2}{\sum_{i=1}^n (a_i - \bar{a})^2}, \quad (8)$$

$$MAE = \frac{\sum_{i=1}^n |p_i - a_i|}{n}, \quad (9)$$

$$RMSE = \sqrt{\frac{\sum_{i=1}^n (p_i - a_i)^2}{n}}, \quad (10)$$

$$RAE = \frac{\sum_{i=1}^n |p_i - a_i|}{\sum_{i=1}^n |\bar{a} - a_i|}. \quad (11)$$

In this formula,  $a_i$  represents the actual output at time  $i$ , and  $p_i$  represents the predicted output at time  $i$ .

### 3. Research Case

#### 3.1. Dataset Description

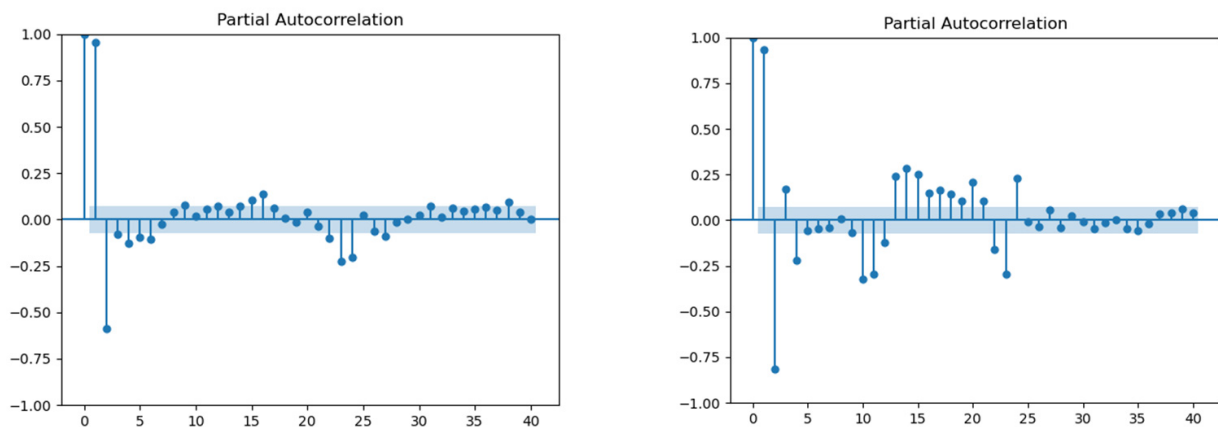
For this study, wind speed and solar irradiance data were collected from clean energy production base sites in the low Yangtze River basin from January 2005 to November 2015. The time intervals for recording both wind speed and solar irradiance were set at 1 h. The base comprises wind turbines with a total capacity of 6767.5 MW and solar units with an ensemble capacity of 8785 MW. Wind and solar power outputs for this region were computed.

#### 3.2. Correlation Analysis

##### 3.2.1. ACF/PACF Results Analysis

In order to select appropriate lag values for our time series forecasting models, we conducted autocorrelation analysis using the Autocorrelation Function (ACF) and Partial Autocorrelation Function (PACF). These analyses help determine the relationship between the current and past power outputs of the clean energy base, specifically focusing on wind and solar power.

The ACF analysis reveals a strong correlation between the clean energy base's wind and solar power output data and the past power outputs. As shown in Figure 4, the PACF verification of the wind power output indicates truncation at lags 2, 23, and 24, with subsequent autocorrelation coefficients falling within insignificant confidence intervals. This truncation indicated a strong predictive relationship at this particular lag, implying that past power outputs at lag 24 had a substantial influence on the current output. Therefore, a lag of 24 was selected for the wind power forecasting model. Similar findings were observed for the solar power output sequence, leading to the choice of a forecasting model with  $L = 24$ .



(a) PACF verification of wind power output (b) PACF verification of solar power output

**Figure 4.** Correlation test of energy output series.

##### 3.2.2. Granger Causality Test Analysis

The Granger causality test requires stationary sequences. Hence, performing an augmented Dickey–Fuller (ADF) test to assess the stationarity of the sequence is essential before utilizing the wind and solar power output sequence data from the clean energy base for forecasting. The specific results of the stationarity test are presented in Table 3:

**Table 3.** Smoothness test of wind and solar output series.

Variable	T	p	Critical Value		
			1%	5%	10%
Wind power output	18.036	0.001	−3.43	−2.862	−2.567
Solar power output	21.615	0.001	−3.43	−2.862	−2.567

The  $p$ -values for wind and solar power output sequences are less than 0.05, indicating that both sequences pass the ADF test for stationarity. The Granger causality test employs a lag of 24. The results are presented in Table 4:

**Table 4.** Grainger causality test of wind and solar output series.

Partnership Samples		F	p
Solar power output	Wind power output	288.101	0.00261
Wind power output	Solar power output	115.041	0.00074

The Granger causality test establishes that the solar power output sequence has a bidirectional causal relationship with the wind power output sequence. The confirmation of bidirectional causality allows the integration of these relationships into the time series forecasting model to enhance forecasting accuracy.

### 3.3. Experimental Design

This study considers the spatiotemporal correlations between wind and solar power and utilizes 11 years of wind and solar power output data from the clean energy base. During the training phase, 80% of the data are used for model parameter learning, whereas the remaining 20% are employed for model validation. Based on the analysis results of the ACF and PACF, the lag step of input features is set to 24, and the forecasting horizon is set to 1 h.

After the successful calibration, the model is applied to forecast wind and solar power output for the next hour. Then, the predicted values are integrated back into the known data for the subsequent round of forecasting. This iterative process is repeated for 24 rounds to obtain day-ahead power output forecasting. The model's performance is evaluated using  $R^2$ , MAE, RMSE, and RAE as accuracy assessment metrics.

#### 3.3.1. Independent Forecasting Approach

In the independent forecasting approach, a single day's wind and solar power outputs are taken as the forecasting targets. Historical data are normalized and fed into the network. However, the instances of zero power output exist within the solar data. These zero values can adversely affect the training of the forecasting model. Therefore, calculating the number of instances with effective solar power output within an hour throughout the day is necessary to address the issue.

The count of daily effective solar power output instances is determined for each month using statistical methods, as depicted in Figure 5:

#### 3.3.2. Ensemble Forecasting Approach

The ensemble forecasting approach involves aggregating the outputs of various energy sources to form a new total output sequence, which is then fed into the forecasting model. In particular, the wind and solar power outputs at a certain time are summed to create a stable total output sequence. Forecasts are obtained for the total output within the day using CNN-LSTM [32]. This method maximizes the complementary nature of different energy sources throughout the day, thereby enhancing forecasting accuracy and stability.

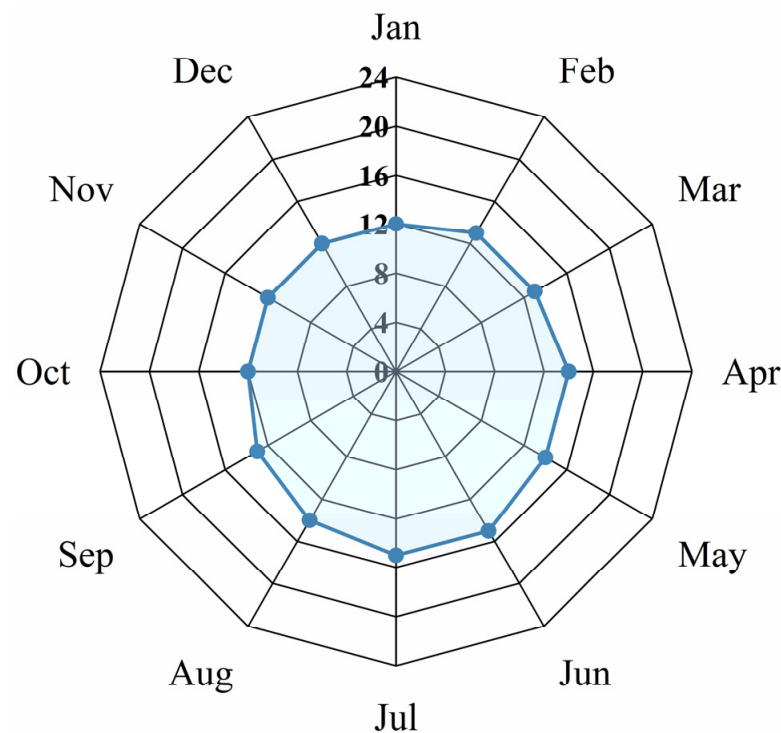


**Figure 5.** Number of hours of effective daily output in each month.

### 3.3.3. Joint Forecasting Approach

When predicting wind and solar power outputs, considering their interdependence can improve forecasting accuracy [33]. In particular, the joint forecasting approach incorporates the past values of both types of output as inputs during the forecasting of one type of output. This approach comprehensively reflects the changing patterns of wind and solar power outputs. Compared with independent forecasting, joint forecasting benefits from the correlation between the two energy sources, considers a broad range of factors, effectively reduces forecasting uncertainty and efficiently supports the operation and management of a power supply system primarily powered by wind and solar energy.

## 4. Result Analysis and Discussion

Twelve representative days are randomly selected for validation to evaluate the forecasting capabilities of the models. The results of different forecasting approaches are compared to determine which method yields accurate forecasts. This aids in choosing the optimal forecasting approach for future use.

### 4.1. Comparison Analysis between Independent and Joint Forecasting

For single-energy source forecasting, independent and joint forecasting approaches can be adopted. The comparative results of their forecasting performances are shown in Figures 6 and 7 and with values shown in Table 5:

**Table 5.** Comparison of forecasting wind and solar output effect.

Forecasting Method	Evaluation Index of Prediction Accuracy			
	R <sup>2</sup> (%)	RAE (%)	RMSE (MW)	MAE (MW)
Independent forecasting of wind power	71.15	39.34	525.7283	373.3667
Joint forecasting of wind power	86.97	29.51	395.2982	275.5099
Independent forecasting of solar power	92.73	17.94	426.5358	232.4478
Joint forecasting of solar power	91.75	18.83	426.0763	243.9843

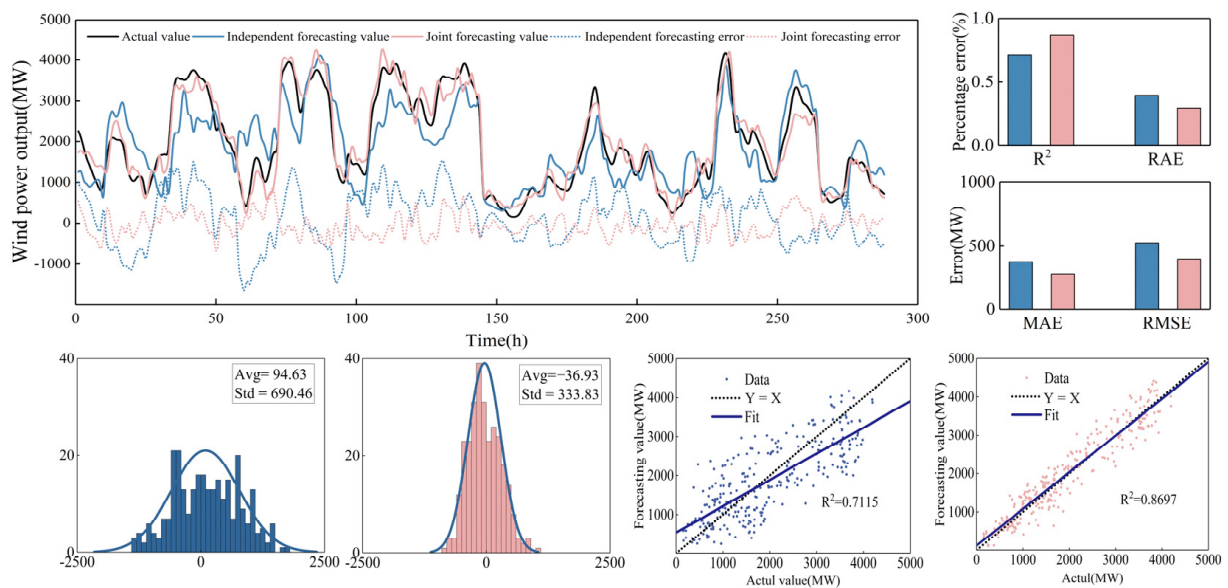


**Figure 6.** Comparison between independent forecasting and joint forecasting of wind power output.

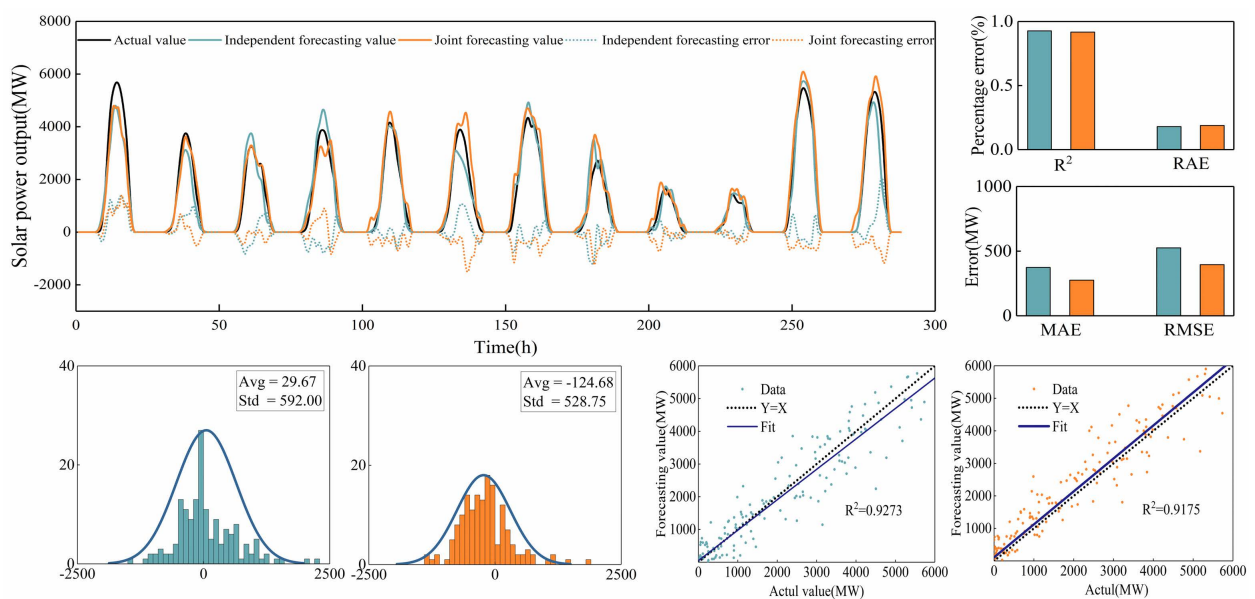


**Figure 7.** Comparison between independent forecasting and joint forecasting of solar output.

Figures 6 and 7 present the visual comparative results between independent and joint forecasting of wind and solar power outputs. The top left corner of the figures displays the comparison between predicted and actual values, along with their errors. The top right corner depicts the histograms of statistical error measurements, including RMSE (MW), MAE (MW), RAE (%), and  $R^2$  (%). The scatter plots showing the error distribution of all models and the linear regression line are displayed at the bottom of the figures.

The calculations show that the joint wind power forecasting approach exhibits small error magnitudes, with all evaluation metrics showing an improvement of more than 20%. The  $R^2$  value for joint wind power forecasting increases by 22.9%, while MAE decreases by 26.2%, RMSE decreases by 24.8%, and RAE decreases by 24.3%. The histograms illustrate that the error distribution of joint wind power forecasting is concentrated, with a great number of error points close to zero. This scenario resembles a more normal distribution. The scatter plots reveal that the joint wind power forecasting approach yields closely distributed results, with the regression line closely aligned with the original data curve.

Compared with independent forecasting, joint wind power forecasting yields superior forecasting outcomes.

Regarding solar power output prediction, both approaches exhibit similar forecasting accuracies and error magnitudes in terms of evaluation metrics. The  $R^2$  metric drops by 1.1%,  $MAE$  increases by 4.96%,  $RMSE$  rises by 4.9%, and  $RAE$  decreases by 4.9%. The prediction errors are primarily concentrated around both sides of zero, and the proximity of the regression line to the original data curve remains consistent. By contrast, the performance of joint solar power output forecasting closely parallels that of independent forecasting.

To further validate the performance of the metric under study, we conducted a Paired-Sample  $t$ -Test to explore the difference between joint prediction errors and independent prediction errors. In the hypothesis test, the null hypothesis ( $H_0$ ) was set as the joint prediction errors being greater than or equal to independent prediction errors ( $\mu d \geq 0$ , where  $\mu d$  represents the difference between joint prediction errors and independent prediction errors), while the alternative hypothesis ( $H_a$ ) indicated that the errors of method A were less than those of method B ( $\mu d < 0$ ). The results of the test are presented in Table 6.

**Table 6.** Paired-Sample  $t$ -Test between joint forecasting and independent forecasting.

Error Type	T-Statistic	$p$ -Value	Testing the Hypothesis $H_0$
Independent forecasting error of wind power output	3.5184	0.0005	Fail
Joint forecasting error of wind power output			
Independent forecasting error of solar power output	4.7104	0.0538	Pass
Joint forecasting error of solar power output			

The results indicate that for wind power output, the  $t$ -statistic is 3.5184 with a corresponding  $p$ -value of 0.0005. It did not pass the significance level  $\alpha$  test (usually  $\alpha = 0.05$ ). For solar power output, the  $T$ -statistic is 4.7104 with a corresponding  $p$ -value of 0.05385, passing the test. This test outcome is consistent with the conclusions drawn from previous computed metrics, providing consistent evidence for our research.

The above results indicate that the joint forecasting approach generally outperforms the independent forecasting approach in predicting wind power outputs. This finding is attributed to the rapid fluctuations in wind power output, influenced by meteorological factors and other variables. Furthermore, this scenario leads to increased volatility. Consequently, solely relying on a single resource as the prediction input may yield suboptimal results. By contrast, the joint forecasting approach comprehensively captures the changing patterns of both wind and solar power outputs, thereby enhancing prediction accuracy.

On the contrary, solar output is relatively stable and changes slowly. Thus, applying the joint forecasting approach to solar power may have limited benefits or even result in a performance worse than that of independent forecasting. In such scenarios, the independent forecasting method may be suitable.

It's important to note that different application scenarios and requirements significantly impact the choice of forecasting methods. Therefore, selecting the appropriate forecasting method should involve a comprehensive consideration of various factors to achieve the best prediction outcomes.

#### 4.2. Comparison Analysis between Independent and Ensemble Forecasting

The aggregated values of independent forecasting must be compared with those of the ensemble forecasting approach to assess the effectiveness of the forecasting methods comprehensively. This analysis aims to examine the differences in accuracy, stability, and other aspects between the two methods. The validation results are shown in Figure 8, with values shown in Table 7. The result of hypothesis test shown in Table 8:

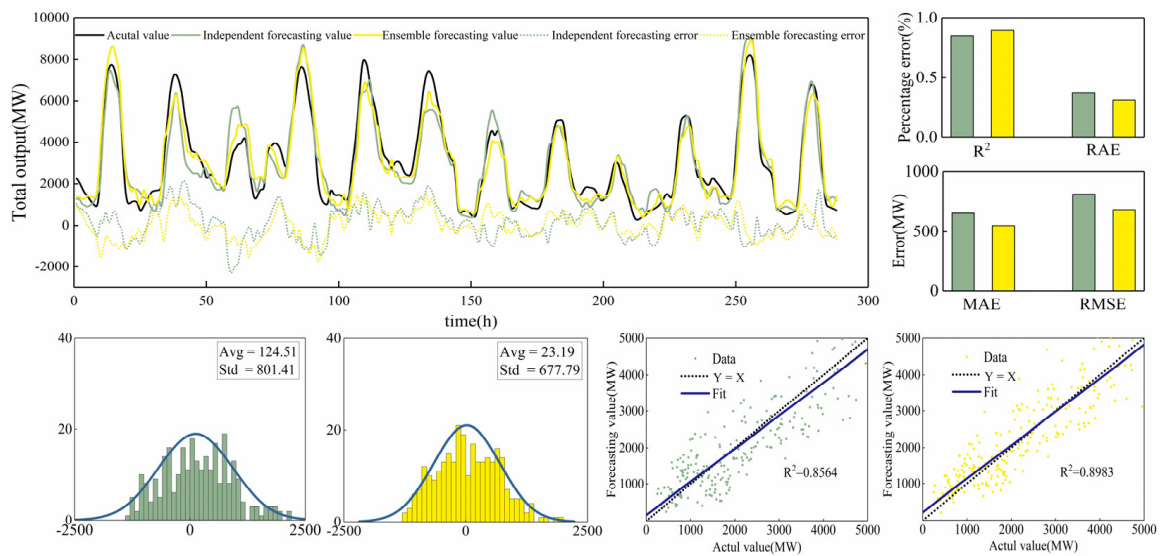


**Figure 8.** Comparison between independent forecasting and ensemble forecasting of wind and solar outputs.

**Table 7.** Comparison of the total output forecasting effect.

Forecasting Method	Forecasting Accuracy Evaluation Index			
	R <sup>2</sup> (%)	RAE (%)	RMSE (MW)	MAE (MW)
Independently forecasting the total output	85.46	36.84	809.6459	649.6335
Ensemble forecasting the total output	89.83	31.13	677.0138	548.9111

**Table 8.** Paired-Sample *t*-Test between ensemble forecasting and independent forecasting.

Error Type	T-Statistic	<i>p</i> -Value	Testing the Hypothesis H0
Independent forecasting error of total output	−2.5389	0.0116	Fail
Joint forecasting error of total output			

Figure 8 demonstrates that adopting the approach of combined forecasting for total output yields significant enhancements in accuracy evaluation metrics. The  $R^2$  value in independent total output forecasting increases from 85.46% to 89.83%, marking a 4.9% improvement. The MAE value in independent total output forecasting decreases from 649.6335 to 548.9111, representing a 15.5% reduction. The RMSE value in independent total output forecasting decreases from 809.6459 to 677.0138, resulting in a 16.5% reduction. The RAE value in independent total output forecasting decreases from 36.84% to 31.13%, showing a 15.5% decrease. Overall, the combined forecasting approach for total output enhances accuracy and precision, particularly in terms of MAE and RMSE, with improvements of approximately 15%. The histograms indicate a uniform distribution of errors in combined forecasting, and the linear fit between the actual and the predicted values is favorable. Furthermore, the value of the *p*-value indicates that the hypothesis that the ensemble forecasting error is greater than or equal to the independent forecasting error did not pass. The result shows that the precision of ensemble forecasting is higher than that of independent forecasting.

In summary, adopting the combined forecasting method allows for a comprehensive utilization of complementarity, error reduction, and prediction accuracy improvement. Our confidence in the effectiveness of this method is bolstered by rigorous validation using random sampling of dates. The consistency of our validation results reaffirms the practical applicability of the combined forecasting approach. While we have discussed the study’s limitations elsewhere, our validation approach minimizes bias and provides robust support

for our conclusions. Ongoing validation efforts and the inclusion of diverse datasets will continue to enhance the reliability and generalizability of our forecasting method.

## 5. Conclusions

This study addressed the wind and solar power output sequences through analyses based on autocorrelation and causal relationships. Independent, ensemble and joint forecasting were conducted to provide a comparative validation analysis and statistical outcomes across four evaluation metrics. The overall conclusions of this study are as follows:

1. Wind and solar power outputs exhibit significant self-correlations and interdependencies. The adoption of ACF and PACF for wind and solar power output sequences verifies the appropriateness of a forecasting model with a lag of 24 for time-series prediction.
2. The accuracy of wind power output time-series prediction is enhanced by incorporating historical solar power output data because of their distinct periodicity and regularity. However, considering historical wind power output data for solar power output time-series prediction can deteriorate forecasting performance because they have high volatility and lack pronounced periodic patterns. Therefore, for power supply systems with a significant presence of wind and solar energy generation, a combined forecasting approach can be employed for wind power output predictions, while the choice of forecasting methods for solar output should be considered based on specific circumstances.
3. Aggregating wind and solar power output sequences for combined forecasting improves accuracy. Given the correlation between wind and solar power output sequences, the total output sequence exhibits great stability and regularity, potentially leading to reduced prediction errors. Moreover, the combined forecasting approach enhances the robustness and stability of predictions by avoiding over-dependence on singular energy data sources. For clean energy bases, adopting combined forecasting for total output utilizing both wind and solar power sequences is reliable and effective.

However, it is important to note that the study has several clear limitations: Firstly, we exclusively considered the complementarity between wind energy and solar energy without including factors related to other renewable energy sources. Future research could expand to the integration of other forms of energy to comprehensively explore issues related to renewable energy integration. Secondly, we did not conduct causality tests for other lag periods, which may limit our comprehensive understanding of the relationship between wind and solar power outputs. Further analysis could encompass broader time series analyses to delve deeper into the causal relationships among these factors. Lastly, our study is built upon a set of assumptions, including idealized models and technical conditions. While these assumptions provided a framework for our analysis, they also imply that our results may be subject to certain limitations in real-world applications. Despite these limitations, our research offers an initial approach to renewable energy integration and provides valuable insights into the complementarity between wind and solar energy. Future research efforts can focus on addressing these limitations and delving further into the integration of renewable energy to enhance sustainability and reliability within the power grid.

**Author Contributions:** Conceptualization, Z.Y. and B.M.; methodology, Z.Y. and B.M.; software, Z.Y.; validation, Z.Y., B.M. and X.Z.; formal analysis, Z.Y.; investigation, Z.Y. and L.T.; resources, Z.Y. and L.T.; data curation, Z.Y. and L.T.; writing—original draft preparation, Z.Y.; writing—review and editing, Z.Y. and B.M.; visualization, Z.Y.; supervision, B.M. and X.Z.; project administration, P.Z.; funding acquisition, P.Z. All authors have read and agreed to the published version of the manuscript.

**Funding:** This work was supported by the Joint Foundation of Shanxi [Grant No. 2019JLP-25], National Natural Science Foundation of China [52009098, U2243216].

**Institutional Review Board Statement:** Not applicable.

**Informed Consent Statement:** Not applicable.

**Data Availability Statement:** Not applicable.

**Conflicts of Interest:** The authors declare no conflict of interest.

## Nomenclature

ACF	Autocorrelation function
PACF	Partial autocorrelation function
L	Lag value
CNN	Convolutional neural network
1D-CNNs	One-dimensional CNNs
LSTM	Long short-term memory
CNN-LSTM	Convolutional neural network–long short-term memory
R <sup>2</sup>	R square
MAE	Mean absolute error
RMSE	Root mean square error
RAE	Relative absolute error

## References

- Cheng, C. Function Remolding of Hydropower Systems for Carbon Neutral and Its Key Problems. *Autom. Electr. Power Syst.* **2021**, *45*, 29–36.
- Zhao, J.; Zhang, G.; Huang, Y. Status and prospect of state estimation for power system containing renewable energy. *Electr. Power Autom. Equip.* **2014**, *34*, 7–20.
- Xie, Y.; Li, C.; Li, M.; Liu, F.; Taukenova, M. An overview of deterministic and probabilistic forecasting methods of wind energy. *iScience* **2023**, *26*, 105804. [[CrossRef](#)] [[PubMed](#)]
- Wang, Y.; Zou, R.; Liu, F.; Zhang, L.; Liu, Q. A review of wind speed and wind power forecasting with deep neural networks. *Appl. Energy* **2021**, *304*, 117766. [[CrossRef](#)]
- Moazzami, M.; Hosseini, S.J.A.D.; Shahinzadeh, H.; Gharehpetian, G.B.; Moradi, J. SCUC Considering Loads and Wind Power Forecasting Uncertainties using Binary Gray Wolf Optimization Method. *Majlesi J. Electr. Eng.* **2018**, *12*, 15–24.
- Zhao, B.; Wang, Y.; Wang, B.; Xuan, W.; Lei, Z.; Ge, L.; Xu, X. Photovoltaic power prediction in distribution network based on ARIMA model time series. *Renew. Energy Resour.* **2019**, *37*, 820–823.
- Wang, J.; Yang, Y.; Wen, D.; Sun, X.; Ren, Z.; Wang, R. A Combined Model of Chaos Prediction of Wind Power Generation Time Series Based on GA-BP and RBF. *Power Syst. Clean Energy* **2022**, *38*, 117–125.
- Heydari, A.; Garcia, D.A.; Keynia, F.; Bisegna, F.; De Santoli, L. A novel composite neural network based method for wind and solar power forecasting in microgrids. *Appl. Energy* **2019**, *251*, 113353. [[CrossRef](#)]
- Zanjani, S.M.; Shahinzadeh, H.; Moradi, J.; Fayaz-dastgerdi, M.H.; Yaici, W.; Benbouzid, M. Short-term Load Forecasting using the Combined Method of Wavelet Transform and Neural Networks Tuned by the Gray Wolf Optimization Algorithm. In Proceedings of the IEEE Global Energy Conference (GEC) 2022, Batman, Turkey, 26–29 October 2022.
- Cui, Y.; Chen, Z.; He, Y.; Xiong, X.; Li, F. An algorithm for forecasting day-ahead wind power via novel long short-term memory and wind power ramp events. *Energy* **2023**, *263*, 125888. [[CrossRef](#)]
- Khan, Z.A.; Hussain, T.; Baik, S.W. Dual stream network with attention mechanism for photovoltaic power forecasting. *Appl. Energy* **2023**, *338*, 120916. [[CrossRef](#)]
- Teferra, D.M.; Ngoo, L.M.; Nyakoe, G.N. Fuzzy-based prediction of solar PV and wind power generation for microgrid modeling using particle swarm optimization. *Heliyon* **2023**, *9*, e12802. [[CrossRef](#)] [[PubMed](#)]
- Liu, H.; Gao, Q.; Ma, P. Photovoltaic generation power prediction research based on high quality context ontology and gated recurrent neural network. *Sustain. Energy Technol. Assess.* **2021**, *45*, 101191. [[CrossRef](#)]
- Wang, K.; Qi, X.; Liu, H. A comparison of day-ahead photovoltaic power forecasting models based on deep learning neural network. *Appl. Energy* **2019**, *251*, 113315. [[CrossRef](#)]
- Yang, X.; Liu, Y.; Xing, G.; Zhang, Y. Method of estimating frequency regulation capacity of wind farm based on wind power probability prediction. *Acta Energetica Solaris Sin.* **2022**, *43*, 409–416.
- Zhang, Z.; Zhang, F.; Yao, W. Day-ahead probabilistic optimal dispatching of source-load-storage system based on probabilistic prediction model of wind power. *Electr. Power Autom. Equip.* **2022**, *42*, 190–197.
- Zhang, Z.; Zhang, F.; Yao, W. Short-term wind power probabilistic forecasting using a new neural computing approach: GMC-DeepNN-PF. *Appl. Soft Comput.* **2022**, *126*, 109247.
- Xue, Y.; Zhang, N.; Yu, Z.; Wu, H.; Li, R. Interval prediction method of wind power based on BiLSTM and Bootstrap. *Renew. Energy Resour.* **2020**, *38*, 1059–1064.

19. Yu, X.; Zhang, W.; Zang, H.; Yang, H. Wind Power Interval Forecasting Based on Confidence Interval Optimization. *Energies* **2018**, *11*, 3336. [[CrossRef](#)]
20. He, Y.; Yan, Y.; Xu, Q. Wind and solar power probability density prediction via fuzzy information granulation and support vector quantile regression. *Int. J. Electr. Power Energy Syst.* **2019**, *113*, 515–527. [[CrossRef](#)]
21. Zhang, J.; Hodge, B.-M.; Florita, A. *Investing the Correlation between Wind and Photovoltaic Power Forecast Errors in the Western Interconnection*; National Renewable Energy Laboratory (NREL): Golden, CO, USA, 2013.
22. Zhang, H.; Cao, Y.; Zhang, Y.; Terzija, V. Quantitative synergy assessment of regional wind-solar energy resources based on MERRA reanalysis data. *Appl. Energy* **2018**, *216*, 172–182. [[CrossRef](#)]
23. Liu, Y.; Wang, H.; Han, S.; Yan, J.; Lu, Z. Real-time Complementarity Evaluation Method for Real-time Complementarity of Wind and Solar Power Considering Their Volatility. *Power Syst. Technol.* **2020**, *44*, 3211–3220.
24. Ren, G.; Wang, W.; Wan, J.; Hong, F.; Yang, K. A novel metric for assessing wind and solar power complementarity based on three different fluctuation states and corresponding fluctuation amplitudes. *Energy Convers. Manag.* **2023**, *278*, 116721. [[CrossRef](#)]
25. Manohar, M.; Koley, E.; Ghosh, S. Microgrid protection under weather uncertainty using joint probabilistic modeling of solar irradiance and wind speed. *Comput. Electr. Eng.* **2020**, *86*, 106684. [[CrossRef](#)]
26. Ramakrishna, R.; Scaglione, A.; Vittal, V.; Dall’Anese, E.; Bernstein, A. A model for joint probabilistic forecast of solar photovoltaic power and outdoor temperature. *IEEE Trans. Signal Process.* **2019**, *67*, 6368–6383. [[CrossRef](#)]
27. Zhang, Y.; Yan, J.; Han, S.; Liu, Y.; Song, Z. Joint forecasting of regional wind and solar power based on attention neural network. In Proceedings of the 2022 IEEE 5th International Electrical and Energy Conference (CIEEC), Nangjing, China, 27–29 May 2022; pp. 4165–4169.
28. Yu, N.; Yi, D.; Tu, X. Analyze Auto-correlations and Partial-correlations Function in time Series. *Math. Theory Appl.* **2007**, *27*, 54–57.
29. Cao, Y. A Comment on Granger Causality Test. *J. Quant. Tech. Econ.* **2006**, *23*, 155–160.
30. Kiranyaz, S.; Avci, O.; Abdeljaber, O.; Ince, T.; Gabbouj, M.; Inman, D.J. 1D convolutional neural networks and applications: A survey. *Mech. Syst. Signal Process.* **2021**, *151*, 107398. [[CrossRef](#)]
31. Liao, X.; Chen, C.; Wu, J. Combined Spatiotemporal Wind Farm Prediction Model Based on CNN-LSTM and Deep Learning. *Inf. Control* **2022**, *51*, 498–512.
32. Ye, L.; Qu, X.; Ma, M.; Yao, Y.; Wang, W.; Zhuang, H.; Dong, L. Multi-energy System Homogeneous Coupling Model Considering Wind-photovoltaic-hydro Power Generations. *Power Syst. Technol.* **2018**, *42*, 158–160.
33. Mao, M.; Zhou, S.; Su, J. Probabilistic Power Flow Forecasting of Microgrid Based on Joint Probability Distribution about Wind and Irradiance. *Trans. China Electrotech. Soc.* **2014**, *29*, 55–63.

**Disclaimer/Publisher’s Note:** The statements, opinions and data contained in all publications are solely those of the individual author(s) and contributor(s) and not of MDPI and/or the editor(s). MDPI and/or the editor(s) disclaim responsibility for any injury to people or property resulting from any ideas, methods, instructions or products referred to in the content.